Reconciling TD-DFT and CASPT2 electronic structure methods for describing the photophysics of DNA

Reconciling TD-DFT and CASPT2 electronic structure methods for describing the photophysics of DNA

Vishal Kumar Jaiswal[a], Mario Taddei[a], Daniel. R Nascimento[b], Marco Garavelli[a], Irene Conti[*a], Artur Nenov[*a]

[a] Dipartimento di Chimica Industriale, Università degli Studi di Bologna, Viale del Risorgimento 4, I-40136 Bologna, Italy, [b] Department of Chemistry, The University of Memphis, Memphis TN 38152, USA.

*(Irene Conti): irene.conti@unibo.it , (Artur Nenov): artur.nenov@unibo.it

ABSTRACT

TD-DFT and CASPT2 are two of the most widely used methods to investigate photoinduced dynamics in DNA based systems. These methods sometimes give diverse dynamics in physiological environments usually modelled by QM/MM protocol. In this work, we demonstrate for the uridine test case that the underlying topology of the potential energy surfaces of electronic states involved in photoinduced relaxation are similar in both electronic structure methods. This is verified by analyzing surface-hopping dynamics performed at the QM/MM level on aqueous solvated uridine at TD-DFT and CASPT2 levels. By constraining the dynamics to remain on $\pi\pi^*$state we observe similar fluctuations in energy and relaxation lifetimes in surface-hopping dynamics in both TD-DFT and experimentally validated CASPT2 methods. This finding calls for a systematic comparison of the ES potential energy surfaces of DNA and RNA nucleosides at the single- and multi-reference levels of theory. The anomalous long excited state lifetime at the TD-DFT level is explained by $n\pi^*$ trapping due to the tendency of TD-DFT in QM/MM schemes with electrostatic embedding to underestimate the energy of the $\pi\pi^*$ state leading to a wrong $\pi\pi^*/n\pi^*$energetic order. A study of the FC energetics suggests that improving the description of surrounding environment through polarizable embedding or by expansion of QM-layer with hydrogen-bonded waters helps restore the correct state order at TD-DFT level.. Thus by combining TDDFT with an accurate modelling of the environment, TD-DFT is positioned as the standout protocol to model photoinduced dynamics in DNA based aggregates and multimers.

INTRODUCTION

The photoinduced dynamics of DNA nucleobases and their nucleosides induced with ultraviolet (UV) light involves the lowest excited states, of $\pi\pi^*$ or $n\pi^*$ nature. It is well known that their energetics is influenced by the surrounding medium, yet the implications with respect to the excited state (ES) deactivation mechanism is still a matter of an intense discussion. Taking Uridine – the RNA counterpart of Thymidine – as an example, while it is generally accepted that the $n\pi^*$ state is the lowest ES in gas-phase, acting as population funnel on the sub-ps time scale and as a doorway to the ns lived triplet manifold,[1–3] there is an ongoing debate regarding its involvement in the ES deactivation in polar media such as DNA's native environment water. This debate is owed to contradicting theoretical findings by time-dependent density functional theory (TD-DFT) [4–8] and multiconfigurational second order perturbation theory (CASPT2)[9–19] – the most widely used approaches for analyzing the electronic structure of nucleobases – regarding the $\pi\pi^*/\ n\pi^*$ energetic order in water. Specifically, CASPT2 predicts a state order inversion with respect to gas-phase, whereas TD-DFT sees the two states quasi degenerate in the Franck-Condon region with the exact order depending on the fine tuning of the computational parameters. Consequently, differing interpretations exist as to the fate of the ES population in condensed phase ranging from a direct ultrafast conversion to the ground state (GS) to trapping in the triplet manifold.[1,3,8,20,21]

TD-DFT, due to its computational economy and "black-box" nature has been widely employed to investigate the electronic structure and relaxation dynamics of DNA nucleobases and their aggregates.[22–26] While being formally exact, in practice TD-DFT, in the commonly employed linear response (LR) formalism (in the following TD-DFT refers to LR-TD-DFT), is

realized in the so called adiabatic local-density approximation (ALDA) which replaces the time-dependent exchange correlation (xc) functional, whose exact mathematical form is unknown, with the time-independent GS xc functional.[27] This prevents orbital relaxation and the LR is applied to the GS orbitals relaxed in the previous DFT calculation. As a consequence, in schemes commonly employed for describing a solute in condensed phase, such as hybrid quantum mechanics (QM) / molecular mechanics (MM) with electrostatic embedding where the environment is represented through a collection of point charges at solvent atomic positions, purely electrostatic solute-solvent interactions are taken into account (point charges enter in the external potential) ES orbitals polarization effects by the electric field generated by the surrounding medium are essentially ignored. This shortcoming can have undesired consequences for the relative energetics of electronic states of different nature in polar solvents. Orbital optimization DFT algorithms such as maximum orbital overlap (MOM)[28] and ΔSCF [29] have been developed to overcome this shortcoming, yet challenges related to variational collapse have so far obstructed application to dynamics simulations.[30]

Variational wavefunction based methods are not prone to the above mentioned issue as they relax orbitals (in the case of CASPT2 this is achieved in the preceding CASSCF step). However, CASPT2 is not a panacea, as it has considerable difficulties to treat at equal footing electronic states with pronounced ionic (such as the $\pi\pi^*$) and covalent (such as the $n\pi^*$) character (in terms of valence-bond theory.[31–35] The dynamical $\sigma - \pi$ polarization in ionic states depends strongly on the active space (AS) size and composition. Studies on nucleobases have evidence the need to use AS going beyond valence π-orbitals.[36,37] As such AS dimensions are unfeasible for dynamics simulations, usually employed full-π AS schemes are prone to errors regarding the

relative energetics of electronic states of different nature, with a different quantitative and even quantitative extent with respect to TD-DFT.

METHODS

The nonadiabatic mixed quantum-classical dynamics at CASPT2/TD-DFT level were performed with a fewest switches Tully surface-hopping algorithm with Tully-Hammes-Schiffer scheme[38] including decoherence corrections.[39] A time-step of 0.5 fs was utilized in surface-hopping dynamics. These nonadiabatic dynamics were conducted with COBRAMM[40–42] interfacing the QM software (OpenMolcas[43]/Gaussian16[44]) with MM software (Amber)[45]. The protocol to generate an optimized QM/MM setup from classical molecular dynamics and further details on surface-hopping dynamics have been previously described.[13] Following the Tully,Hammes-Schiffer scheme the time-derivative coupling between two electronic states is related to the overlap integrals between the adiabatic wavefunctions at successive time-steps. These overlap integrals were computed through RASSI module in OpenMolcas for CASPT2 surface-hopping dynamics. For surface-hopping dynamics at TD-DFT level, time-derivative coupling between the lowest two excited-states were computed at the TD-DFT level with the Tamm-Damcoff approximation with a procedure recently proposed by some of us for the fast and efficient computation of wavefunction overlaps relying on a unitary transformation of the MO overlap matrix.[46] Since these procedure only works for estimating the coupling between excited-states at TD-DFT level, the return to ground-state was assumed when the energy-gap between the active-state and ground-state was less then 0.5 eV. For the set of TD-DFT dynamics constrained to remain on pipi* state, the dynamics was forced to remain on the excited electronic

state which has the largest transition-dipole moment for transition from ground-state to the lowest two excited-states at every time step.

The multiconfigurational QM computations were done at XMS-CASPT2 level with an underlying CASSCF wavefunction state-averaged over 9 states with an active space of 14 electrons in 10 orbitals consisting of 8 valence pi/pi* orbitals and two lone pairs while employing an ANO-L-VDZP basis-set. An IPEA shift of 0.0 and imaginary shift of 0.2 were used. The TD-DFT QM computations were done with the CAM-B3LYP functional employing the Pople split-valence 6-311G(d,p) basis-set.

For the comparison of vertical transition energies in various embedding schemes, Gaussian16 was utilized for electrostatic embedding and PCM computations. The polarizable embedding computations were done with Dalton.[47] The embedding potentials for solvent was generated using the PyFrame package.[48] The embedding parameters consisting of point charges, multipole moments and polarizability for water were generated by PyFrame and are described in reference.[49]

RESULTS AND DISCUSSION

The consequence for ES nonadiabatic dynamics due to the disparity between TD-DFT and CASPT2 in modelling the electronic structure of DNA nucleobases is exemplified for water solvated Uridine. Figure 1 compares the evolution of the energy gap between ground and active state along on-the-fly Tully fewest switches surface hopping (FSSH) dynamics simulations performed with both methodologies on a swarm of 59 trajectories with the same initial conditions initialized in the bright $\pi\pi^*$ state. These dynamics are carried out in a QM/MM model

of the solvated system where the chromophore (nucleobase) is computed at the QM level and the sugar and water molecules are described by MM force fields and point-charges. The TD-DFT/MM setup considers the lowest two excited states and employs the Tamm-Dancoff approximation (TDA), which gives access to approximate non-adiabatic couplings between the excited states.[50] It is well known that TD-DFT has convergence issues in the vicinity of GS/ES conical intersection (CI) seam. However, this does not pose a restriction since the focus of this study is to track the time needed to reach the CI seam. Thus, the dynamics have been interrupted when the energy gap falls below 0.5 eV assuming that reaching the CI is eminent. In the passing we note TD-DFT flavors such as spin-flip which use an electronic configuration different from the GS closed shell one as a reference (e.g. a high-spin triplet configuration) which allows to describe correctly internal conversion to the GS.[51–53] The CASPT2 set up employs an AS of 14 electrons in 10 orbitals comprising all frontier valence π-orbitals, as well as the oxygen lone pairs. Nine states are included in the state-averaging procedure. The second-order perturbational correction to the CASSCF wavefunction is done by employing the extended multistate version (XMS-CASPT2) which ensures smooth potential energy surfaces in regions of degenerate electronic levels. Further details are provided in the Methodology.

A clear difference in the excited state behavior of uracil at the CASPT2 or TDDFT level is documented in Figure 1, where in the first 200 fs the average energy gap between the fundamental state and the active excited state is noticeably larger in the case of the single reference method. In the XMS-CASPT2 ensemble, more than half (35) of the trajectories hop to the GS within 200 fs. The rapid decrease in the GS-active state energy gap in the course of the dynamics is indicative of a ballistic motion on the ES potential energy surface (PES) towards the ES/GS CI seam. In the TD-DFT ensemble only 12 trajectories approach the ES/GS CI seam

in the first 200 fs, the population is trapped in the ES preventing the ballistic decay resulting in the larger and longer living average energy gap of the active-state with the GS (Figure 1b). A closer inspection of the CASPT2 dynamics evidences the secondary role of the $n\pi^*$ state in the deactivation dynamics, collecting only about 10% of the ES population. Instead, as shown in Figure 1c, the dynamics at the TD-DFT level involves a high participation of the $n\pi^*$ state. It has been documented that the $n\pi^*$ state does not show a low lying CI with the GS which prevents ultrafast decay and leads to the longer ES lifetime reported.[11]

It is highly desirable to understand the underlying reason for the different dynamics predicted by TD-DFT and XMS-CASPT2. It is reasonable to ask whether the shortcomings of the two methods in describing the relative energetics of the $\pi\pi^*$ and $n\pi^*$ states affect also the topology of the ES PES, in particular with regard to barriers and CI seam accessibility. What makes things even more interesting is the recent validation of the CASPT2 dynamics by UV/Vis transient absorption spectroscopy experiments with high (sub-30 fs) temporal resolution which see the ES signals decay on the 100 fs timescale[13] , posing the question of error mitigation / compensation at the CASPT2 level. It is, therefore, not surprising that in the past extensive static studies have been dedicated to the comparison of TD-DFT and CASPT2 energetics at stationary points on the ES PES .[54,55]

In this communication we undertake a different route by engineering a dynamical approach aimed at comparing the topologies of the PES. Specifically, we re-run the on-the-fly dynamics using, on the one side SS-CASPT2 with an AS of 10 electrons in 8 orbitals comprising only valence π-orbitals (thus excluding oxygen lone pairs) and on the other side TD-DFT forcing the active state to always coincide with the bright state. In this way we enforce the dynamics to evolve on the $\pi\pi^*$ PES and can assess if and when the trajectories diverge. The results of these

{QM}/force-$\pi\pi^*$ trajectories are shown in Figure 2a and compared to the unbiased XMS-CASPT2/TD-DFT trajectories presented in Figure 1 (All the 29 trajectories with the population constrained to remain on $\pi\pi^*$ state at SSCASPT2/TDDFT are shown in Figure S1). Interestingly, the {QM}/force-$\pi\pi^*$ trajectories show similar average decay time to the GS as the ones run at the XMS-CASPT2 level, regardless of the QM-method used. The similar behavior of TD-DFT and CASPT2 dynamics, once the $n\pi^*$ is taken out of the picture, clearly demonstrates that the $\pi\pi^*$ PES predicted by both methods have very similar, if not identical, topologies. This can be further appreciated in Figure 3 showing two unbiased TD-DFT trajectories, one which hops to the GS (Figure 3a-c) and a second one which remains trapped in ES (Figure 3d-f). When the unbiased trajectory decays to the GS (Figure 3d, dashed lines), the involvement of the $n\pi^*$ state is minimal – as can be seen by examining the oscillator strength of the active state – and the system ballistically moves on the $\pi\pi^*$ state towards the ES/GS CI seam. In this case, both unbiased and the {QM}/force-$\pi\pi^*$ TD-DFT dynamics hop to the GS through a similar CI structure as encountered in the unbiased XMS-CASPT2 dynamics (Figure 3f). Instead, when the unbiased TD-DFT remains trapped in the ES (Figure 3d-f) this is clearly due to the involvement of the $n\pi^*$ state manifested in the almost zero oscillator strength of the active state (Figure 3b). When the TD-DFT dynamics is constrained to remain on the $\pi\pi^*$ state (Figure 3a, dotted line), the decay to the GS occurs on the same sub-100 fs time scale (Figure 3a, solid line) and through a similar CI structure (Figure 3c) as encountered in the unbiased XMS-CASPT2 dynamics.

The above behavior is encountered for all trajectories with only a few outliers which remain trapped in the ES at the {QM}/force-$\pi\pi^*$ level and eventually slowly diverge on the timescale of several hundred fs. This suggests that the different relative energetics of the $\pi\pi^*$/ $n\pi^*$ states

189 is the responsible for the erroneous behavior of TD-DFT/MM trajectories. Indeed, as shown in
190 Figure 2b, which reports the distribution of transition energies to the $\pi\pi^*$ and $n\pi^*$ states for a
191 Wigner sampled ensemble of geometries around the GS equilibrium, the $\pi\pi^*$ is destabilized and
192 lies on average 0.5 eV *above* the $n\pi^*$ state at the TD-DFT level, whereas it lies 0.5 eV *below*
193 the $n\pi^*$ state at the XMS-CASPT2 level. (Similar trends are seen also for DFT functionals
194 wb97xd and LC-wHPBE shown in Figure S2.) Notably, the $n\pi^*$ state shows little variation
195 between the two levels peaking around 5 eV. The nearly 1 eV variation of the $\pi\pi^*$ energetics
196 explains why the CASPT2 trajectories (both unbiased and force- $\pi\pi^*$) decay to the GS with
197 minimal involvement of $n\pi^*$ state while the unbiased TD-DFT trajectories end up in the $n\pi^*$
198 state.

199 Hence, to confidently use TD-DFT to investigate photoinduced dynamics in DNA-based
200 systems in an explicit environment, a suitable strategy is needed to obtain the correct ES
201 energetic order. To address this issue, we compare different TD-DFT schemes for representing
202 the solute-solvent interaction in the Franck Condon region. A 0.3 eV red-shift of the $\pi\pi^*$ state
203 from gas-phase (5.08 eV)[56] to solvent (4.79 eV)[57] has been established experimentally. The
204 energy of the $n\pi^*$ state is only known in solution (5.17 eV)[58] but firm theoretical evidence
205 suggest it peaks around 4.8 eV in gas-phase.[59,60] This implies a 0.4 eV blue-shift of the $n\pi^*$ from
206 gas-phase to solvent, concomitant to state-order inversion.

207 There are increasing degrees of sophistication utilized within the QM/MM formalism to
208 simulate the effect of the environment acting on the chromophore. In electrostatic embedding
209 (EE) schemes the environment is described as a collection of n-th order multipoles. Usually,
210 only the zeroth-order multipole i.e. just a collection point charges at solvent atomic positions are
211 used. When these multipoles are also augmented by a polarizability tensor this leads to the

polarizable embedding (PE) scheme, which allows one to describe the response of the solvent charge density to the solute electron density.[61–64]

In Table 1 we present the effect of EE and PE QM(TD-DFT)/MM strategies on the energetic order of the lowest $\pi\pi^*/\, n\pi^*$ states in solvated Uridine at Franck-Condon geometry. To enable comparison between the two MM models the entire solute (i.e. sugar + nucleobase) was included in the QM layer[1]. In gas-phase the $\pi\pi^*$ state (5.2 eV) is above the $n\pi^*$ state (4.8 eV), in excellent agreement with the experimental findings. As seen in Table 1, water treated at the EE level reproduces the hypsochromic shift of the $n\pi^*$ state but not the bathochromic shift of the $\pi\pi^*$ state leading to a significantly underestimated $\pi\pi^*/\, n\pi^*$ gap. In fact, the EE does not succeed in reproducing the state order inversion placing the $n\pi^*$ state below $\pi\pi^*$ state even in water. On the other hand, the PE scheme corrects the order of the two states placing $n\pi^*$ state above the $\pi\pi^*$ state, however, it underestimates the splitting. We conducted additional tests by expanding the QM-region to include the nearest solvent molecules (shown in Figure S3) following previous works on solvated uracil that reported improved solvatochromic shifts.[4] However, as shown in Table 1, this doesn't significantly improve the excitation energies in our setup.

Continuum solvent models like the polarization continuum model (PCM) offer an alternative for describing homogeneous isotropic environments avoiding the need to simulate solvent distributions a priori through molecular dynamics. The solvent electric field is partitioned into a slow inertial part and a fast polarization part which can respond instantly to changes in solute electron density rearrangement following vertical excitation. In the zeroth-order approximation the vertical transition energies are computed in the reaction field equilibrated to the GS density.

[1] As demonstrated in the SI with the EE scheme, having the sugar inside or outside the QM layer does not affect the energetics. The decision to add it in the QM layer is practical as this set up requires to compute the polarizability tensor only for the solvent. Moreover, it allows for employing continuum models around the QM region as discussed below.

The linear response of the fast polarization can be computed either by the interaction to the transition density (PCM-LR) or to the difference density (PCM-cLR) of the initial and final states involved in the vertical transition.[65] As it has been appreciated that these corrections describe two different physical interactions, dispersion and state-specific polarization, it has been suggested the two corrections can be added to zeroth order response as done in cLR2 protocol.[66]

In Table 1 we report the effect of QM(TD-DFT)/PCM strategies on the energetic order of the lowest $\pi\pi^*$ and $n\pi^*$ states. It becomes evident that the PCM succeeds in obtaining the correct order once the QM-region is expanded to include nearest solvent molecules with outcome comparable to the QM(TD-DFT)/MM(PE) scheme. The protocol of an expanded QM region combined with PCM-LR has been demonstrated previously to reproduce the maxima of experimental linear absorption spectra[4,67,68] , yet PCM, in its time-independent implementation, cannot account for the dynamic solvent response, it either keeps the slow component unrelaxed or allows it to fully adapt to the ES electronic density, representative of ES solvent equilibration.[69] With the ongoing developments in the time-dependent extension of PCM framework, it is becoming possible to employ the PCM solvent scheme also in dynamics simulations.[70]

Table 1 emphasizes that the energy of the $\pi\pi^*$ state is significantly overestimated in water with all TD-DFT based solvation schemes. *None* of the reported strategies are able to reproduce the 0.3 eV bathochromic shift in aqueous solution, the correct state order is rather realized by acting on the $n\pi^*$ state. Whereas the interaction of $n\pi^*$ state with the solvent is mainly electrostatic in nature and, thus, accessible to MM and PCM schemes within the ALDA LR

255 formalism, the interaction of $\pi\pi^*$ state is more subtle and due to mutual solute-solvent
256 polarization effects.[71,72]

257 As noted earlier, wavefunction based methods, despite being capable to treating states of
258 different nature, are not immune to problems with respect to state ordering. The CASPT2
259 method shows a tendency to overstabilize the $\pi\pi^*$ state due to overestimation of the local
260 electronic correlation in the σ-manifold omitted at the underlying variational CASSCF level
261 with AS comprising only valence π-orbitals. In gas-phase, accurate energies at the CASPT2
262 level have been obtained by an intricate procedure involving expanded AS containing extra-
263 valence orbitals, diffuse basis sets and correction of valence-Rydberg mixing.[36,37,73] Specifically,
264 a blue-shift of 0.25 eV (from 4.95 to 5.20 eV) has been reported in going from (10,8) AS to
265 (0,0|10,8|2,12) RAS expanded with 12 additional extra-valence orbitals in RAS3 and allowing
266 up to double excitations therein, with the converged energy, closely matching other high-level
267 wavefunction based computations[60] . While the issue of valence-Rydberg mixing is largely
268 absent in QM/MM protocols, an expanded active space is still needed to match the linear
269 absorption of nucleobases/nucleotides in aqueous solvents.[13] However, large AS are not feasible
270 for on-the-fly non-adiabatic dynamics and the commonly utilized AS comprising of only frontier
271 orbitals (e.g. AS(10,8) or AS(14,10)) have the tendency to strongly overestimate the
272 bathochromic shift of the $\pi\pi^*$ by 0.3-0.4 eV[13] placing it at 4.4-4.5 eV[2]. This suggests
273 overestimation of the $\pi\pi^*$ involvement in solution, in stark contrast to TD-DFT. It bears noting,
274 however, that the $n\pi^*$ state is also underestimated with AS(10,8) or AS(14,10), so that the $\pi\pi^*$-
275 $n\pi^*$ energy gap remain 0.4 eV independent of the AS dimension. This is the reason for the

[2] The value corresponds to the maximum of the $\pi\pi^*$ absorption band obtained from Wigner sampling 500 water solvated geometries around the GS equilibrium.

agreement between experimental and simulated transient absorption spectra based on QM(CASPT2)/MM(EE). Nevertheless, one needs to be judicious when assessing the relative $\pi\pi^*/\ n\pi^*$ energetics in systems where the interplay between these states is supposed to play an active role in relaxation.[54,74] We advise to benchmark the modest ASs usually employed in on-the-fly dynamics against ASs expanded beyond valence orbitals.

CONCLUSIONS

In this work we have undertaken a critical assessment of two commonly used methods TD-DFT and CASPT2 to describe non-adiabatic dynamics of DNA/RNA based systems in QM/MM setup. Utilizing a case study of aqueous solvated Uridine, we show that TD-DFT and CASPT2 predict very similar topologies of the PES of the lowest $\pi\pi^*$ state. Dynamics confined to the $\pi\pi^*$ PES run with both methodologies exhibit ultrafast internal conversion to the GS through coinciding CI and matching lifetimes. The culprit for the discrepant behavior of TD-DFT/MM dynamics compared to the experimentally validated CASPT2/MM is merely the different relative energetics of the $\pi\pi^*$ and $n\pi^*$ states in the QM/MM setup. In particular, LR-TD-DFT in an electrostatic embedding setup does not succeed in describing the bathochromic shift of the $\pi\pi^*$ state leading to overestimation of the $n\pi^*$ involvement and, consequently, to artificially inflated ES lifetimes. We show that the issues can be mitigated at TD-DFT/MM level by improving the description of the environment through two different strategies: (a) at the QM/MM level using the polarizable embedding (b) with PCM when hydrogen-bonded solvent molecules are treated that the QM level. (see Table1)

We hope that recognizing the accord between LR-TD-DFT and CASPT2 in describing the PES of the photoactive state is a step towards resolving the long standing debate in the community. As CASPT2 is not practical for performing on-the-fly dynamics in extended DNA fragments, improving DFT to better capture the solvatochromic shifts of the protagonist states in the IC of the nucleobases will help position DFT as the stand out protocol for studying DNA photophysics. Moreover, it will pave the way for exciting prospects such as the development of hybrid schemes in which CASPT2 is used on top of LR-TD-DFT on-the-fly dynamics to compute quantities not easily accessible to LR methods – e.g. states with pronounced double excitation character – which are of interest for nonlinear spectroscopies.

SUPPLEMENTARY MATERIALS

Table S1 and Figure S1 and S2 along with solvent parameters utilized for electrostatic and polarizable embedding computations can be found at XXXX

REFERENCES

(1) Yu, H.; Sanchez-Rodriguez, J. A.; Pollum, M.; Crespo-Hernández, C. E.; Mai, S.; Marquetand, P.; González, L.; Ullrich, S. Internal Conversion and Intersystem Crossing

Pathways in UV Excited, Isolated Uracils and Their Implications in Prebiotic Chemistry. *Phys. Chem. Chem. Phys.* **2016**, *18* (30), 20168–20176. https://doi.org/10.1039/C6CP01790H.
(2) Chakraborty, P.; Liu, Y.; Weinacht, T.; Matsika, S. Effect of Dynamic Correlation on the Ultrafast Relaxation of Uracil in the Gas Phase. *Faraday Discuss.* **2021**, *228* (0), 266–285. https://doi.org/10.1039/D0FD00110D.
(3) Richter, M.; Mai, S.; Marquetand, P.; González, L. Ultrafast Intersystem Crossing Dynamics in Uracil Unravelled by Ab Initio Molecular Dynamics. *Phys. Chem. Chem. Phys.* **2014**, *16* (44), 24423–24436. https://doi.org/10.1039/C4CP04158E.
(4) Improta, R.; Barone, V. Absorption and Fluorescence Spectra of Uracil in the Gas Phase and in Aqueous Solution: A TD-DFT Quantum Mechanical Study. *J. Am. Chem. Soc.* **2004**, *126* (44), 14320–14321. https://doi.org/10.1021/ja0460561.
(5) Improta, R.; Barone, V. PCM/TD-DFT Study of the Two Lowest Excited States of Uracil Derivatives in Solution: The Effect of the Functional and of the Cavity Model. *Journal of Molecular Structure: THEOCHEM* **2009**, *914* (1), 87–93. https://doi.org/10.1016/j.theochem.2009.02.021.
(6) Zhang, X.; Herbert, J. M. Excited-State Deactivation Pathways in Uracil versus Hydrated Uracil: Solvatochromatic Shift in the 1nπ* State Is the Key. *J. Phys. Chem. B* **2014**, *118* (28), 7806–7817. https://doi.org/10.1021/jp412092f.
(7) Conti, I.; Martínez-Fernández, L.; Esposito, L.; Hofinger, S.; Nenov, A.; Garavelli, M.; Improta, R. Multiple Electronic and Structural Factors Control Cyclobutane Pyrimidine Dimer and 6–4 Thymine–Thymine Photodimerization in a DNA Duplex. *Chemistry – A European Journal* **2017**, *23* (60), 15177–15188. https://doi.org/10.1002/chem.201703237.
(8) Improta, R.; Santoro, F.; Blancafort, L. Quantum Mechanical Studies on the Photophysics and the Photochemistry of Nucleic Acids and Nucleobases. *Chemical Reviews* **2016**, *116* (6), 3540–3593. https://doi.org/10.1021/acs.chemrev.5b00444.
(9) Yamazaki, S.; Taketsugu, T. Nonradiative Deactivation Mechanisms of Uracil, Thymine, and 5-Fluorouracil: A Comparative Ab Initio Study. *J. Phys. Chem. A* **2012**, *116* (1), 491–503. https://doi.org/10.1021/jp206546g.
(10) Bistafa, C.; Georg, H. C.; Canuto, S. Combining Ab Initio Multiconfigurational and Free Energy Gradient Methods to Study the π–Π* Excited State Structure and Properties of Uracil in Water. *Computational and Theoretical Chemistry* **2014**, *1040–1041*, 312–320. https://doi.org/10.1016/j.comptc.2014.04.024.
(11) Pepino, A. J.; Segarra-Martí, J.; Nenov, A.; Rivalta, I.; Improta, R.; Garavelli, M. UV-Induced Long-Lived Decays in Solvated Pyrimidine Nucleosides Resolved at the MS-CASPT2/MM Level. *Phys. Chem. Chem. Phys.* **2018**, *20* (10), 6877–6890. https://doi.org/10.1039/C7CP08235E.
(12) Pepino, A. J.; Segarra-Martí, J.; Nenov, A.; Improta, R.; Garavelli, M. Resolving Ultrafast Photoinduced Deactivations in Water-Solvated Pyrimidine Nucleosides. *J. Phys. Chem. Lett.* **2017**, *8* (8), 1777–1783. https://doi.org/10.1021/acs.jpclett.7b00316.
(13) Borrego-Varillas, R.; Nenov, A.; Kabaciński, P.; Conti, I.; Ganzer, L.; Oriana, A.; Jaiswal, V. K.; Delfino, I.; Weingart, O.; Manzoni, C.; Rivalta, I.; Garavelli, M.; Cerullo, G. Tracking Excited State Decay Mechanisms of Pyrimidine Nucleosides in Real Time. *Nature Communications* **2021**, *12* (1), 7285. https://doi.org/10.1038/s41467-021-27535-7.
(14) Kabaciński, P.; Romanelli, M.; Ponkkonen, E.; Jaiswal, V. K.; Carell, T.; Garavelli, M.; Cerullo, G.; Conti, I. Unified Description of Ultrafast Excited State Decay Processes in

Epigenetic Deoxycytidine Derivatives. **2021**, 11070–11077. https://doi.org/10.1021/acs.jpclett.1c02909.
(15) Conti, I.; Nenov, A.; Höfinger, S.; Flavio Altavilla, S.; Rivalta, I.; Dumont, E.; Orlandi, G.; Garavelli, M. Excited State Evolution of DNA Stacked Adenines Resolved at the CASPT2//CASSCF/Amber Level: From the Bright to the Excimer State and Back. *Phys. Chem. Chem. Phys.* **2015**, *17* (11), 7291–7302. https://doi.org/10.1039/C4CP05546B.
(16) Conti, I.; Garavelli, M. Evolution of the Excitonic State of DNA Stacked Thymines: Intrabase Ππ* → S0 Decay Paths Account for Ultrafast (Subpicosecond) and Longer (>100 Ps) Deactivations. *J. Phys. Chem. Lett.* **2018**, *9* (9), 2373–2379. https://doi.org/10.1021/acs.jpclett.8b00698.
(17) Conti, I.; Garavelli, M.; Orlandi, G. Deciphering Low Energy Deactivation Channels in Adenine. *J. Am. Chem. Soc.* **2009**, *131* (44), 16108–16118. https://doi.org/10.1021/ja902311y.
(18) Conti, I.; Altoè, P.; Stenta, M.; Garavelli, M.; Orlandi, G. Adenine Deactivation in DNA Resolved at the CASPT2//CASSCF/AMBER Level. *Phys. Chem. Chem. Phys.* **2010**, *12* (19), 5016–5023. https://doi.org/10.1039/B926608A.
(19) Giussani, A.; Conti, I.; Nenov, A.; Garavelli, M. Photoinduced Formation Mechanism of the Thymine–Thymine (6–4) Adduct in DNA; a QM(CASPT2//CASSCF):MM(AMBER) Study. *Faraday Discuss.* **2018**, *207* (0), 375–387. https://doi.org/10.1039/C7FD00202E.
(20) Barbatti, M.; Aquino, A. J. A.; Szymczak, J. J.; Nachtigallová, D.; Hobza, P.; Lischka, H. Relaxation Mechanisms of UV-Photoexcited DNA and RNA Nucleobases. *Proceedings of the National Academy of Sciences* **2010**, *107* (50), 21453–21458. https://doi.org/10.1073/pnas.1014982107.
(21) Brister, M. M.; Crespo-Hernández, C. E. Excited-State Dynamics in the RNA Nucleotide Uridine 5′-Monophosphate Investigated Using Femtosecond Broadband Transient Absorption Spectroscopy. *J. Phys. Chem. Lett.* **2019**, *10* (9), 2156–2161. https://doi.org/10.1021/acs.jpclett.9b00492.
(22) Ibele, L. M.; Sánchez-Murcia, P. A.; Mai, S.; Nogueira, J. J.; González, L. Excimer Intermediates En Route to Long-Lived Charge-Transfer States in Single-Stranded Adenine DNA as Revealed by Nonadiabatic Dynamics. *J. Phys. Chem. Lett.* **2020**, *11* (18), 7483–7488. https://doi.org/10.1021/acs.jpclett.0c02193.
(23) Banyasz, A.; Martínez-Fernández, L.; Balty, C.; Perron, M.; Douki, T.; Improta, R.; Markovitsi, D. Absorption of Low-Energy UV Radiation by Human Telomere G-Quadruplexes Generates Long-Lived Guanine Radical Cations. *J. Am. Chem. Soc.* **2017**, *139* (30), 10561–10568. https://doi.org/10.1021/jacs.7b05931.
(24) Martinez-Fernandez, L.; Changenet, P.; Banyasz, A.; Gustavsson, T.; Markovitsi, D.; Improta, R. Comprehensive Study of Guanine Excited State Relaxation and Photoreactivity in G-Quadruplexes. *J. Phys. Chem. Lett.* **2019**, *10* (21), 6873–6877. https://doi.org/10.1021/acs.jpclett.9b02740.
(25) Mantela, M.; Morphis, A.; Lambropoulos, K.; Simserides, C.; Di Felice, R. Effects of Structural Dynamics on Charge Carrier Transfer in B-DNA: A Combined MD and RT-TDDFT Study. *J. Phys. Chem. B* **2021**, *125* (16), 3986–4003. https://doi.org/10.1021/acs.jpcb.0c11489.
(26) Shepard, C.; Zhou, R.; Yost, D. C.; Yao, Y.; Kanai, Y. Simulating Electronic Excitation and Dynamics with Real-Time Propagation Approach to TDDFT within Plane-Wave

Pseudopotential Formulation. *The Journal of Chemical Physics* **2021**, *155* (10), 100901. https://doi.org/10.1063/5.0057587.
(27) Elliott, P.; Furche, F.; Burke, K. Excited States from Time-Dependent Density Functional Theory. In *Reviews in Computational Chemistry*; Reviews in Computational Chemistry; 2008; pp 91–165. https://doi.org/10.1002/9780470399545.ch3.
(28) Gilbert, A. T. B.; Besley, N. A.; Gill, P. M. W. Self-Consistent Field Calculations of Excited States Using the Maximum Overlap Method (MOM). *J. Phys. Chem. A* **2008**, *112* (50), 13164–13171. https://doi.org/10.1021/jp801738f.
(29) Gavnholt, J.; Olsen, T.; Engelund, M.; Schiøtz, J. $\ensuremath{\Delta}$ Self-Consistent Field Method to Obtain Potential Energy Surfaces of Excited Molecules on Surfaces. *Phys. Rev. B* **2008**, *78* (7), 075441. https://doi.org/10.1103/PhysRevB.78.075441.
(30) Hait, D.; Head-Gordon, M. Orbital Optimized Density Functional Theory for Electronic Excited States. *J. Phys. Chem. Lett.* **2021**, *12* (19), 4517–4529. https://doi.org/10.1021/acs.jpclett.1c00744.
(31) Kimber, P.; Plasser, F. Toward an Understanding of Electronic Excitation Energies beyond the Molecular Orbital Picture. *Phys. Chem. Chem. Phys.* **2020**, *22* (11), 6058–6080. https://doi.org/10.1039/D0CP00369G.
(32) Roos, B. O.; Andersson, K.; Fülscher, M. P. Towards an Accurate Molecular Orbital Theory for Excited States: The Benzene Molecule. *Chemical Physics Letters* **1992**, *192* (1), 5–13. https://doi.org/10.1016/0009-2614(92)85419-B.
(33) Davidson, E. R. The Spatial Extent of the V State of Ethylene and Its Relation to Dynamic Correlation in the Cope Rearrangement. *J. Phys. Chem.* **1996**, *100* (15), 6161–6166. https://doi.org/10.1021/jp952794n.
(34) Angeli, C. On the Nature of the $\pi \rightarrow \Pi^*$ Ionic Excited States: The V State of Ethene as a Prototype. *Journal of Computational Chemistry* **2009**, *30* (8), 1319–1333. https://doi.org/10.1002/jcc.21155.
(35) Michl, J.; Klessinger, M. *Excited States and Photochemistry of Organic Molecules*; VCH Publishers Inc.: New York, 1995.
(36) Nenov, A.; Giussani, A.; Segarra-Martí, J.; Jaiswal, V. K.; Rivalta, I.; Cerullo, G.; Mukamel, S.; Garavelli, M. Modeling the High-Energy Electronic State Manifold of Adenine: Calibration for Nonlinear Electronic Spectroscopy. *The Journal of Chemical Physics* **2015**, *142* (21), 212443. https://doi.org/10.1063/1.4921016.
(37) Nenov, A.; Mukamel, S.; Garavelli, M.; Rivalta, I. Two-Dimensional Electronic Spectroscopy of Benzene, Phenol, and Their Dimer: An Efficient First-Principles Simulation Protocol. *J. Chem. Theory Comput.* **2015**, *11* (8), 3755–3771. https://doi.org/10.1021/acs.jctc.5b00443.
(38) Hammes-Schiffer, S.; Tully, J. C. Proton Transfer in Solution: Molecular Dynamics with Quantum Transitions. *The Journal of Chemical Physics* **1994**, *101* (6), 4657–4667. https://doi.org/10.1063/1.467455.
(39) Tully, J. C. Molecular Dynamics with Electronic Transitions. *The Journal of Chemical Physics* **1990**, *93* (2), 1061–1071. https://doi.org/10.1063/1.459170.
(40) Weingart, O.; Nenov, A.; Altoè, P.; Rivalta, I.; Segarra-Martí, J.; Dokukina, I.; Garavelli, M. COBRAMM 2.0 — A Software Interface for Tailoring Molecular Electronic Structure Calculations and Running Nanoscale (QM/MM) Simulations. *Journal of Molecular Modeling* **2018**, *24* (9), 271. https://doi.org/10.1007/s00894-018-3769-6.

(41) Avagliano, D.; Conti, I.; El-Tahawy, M. M. T.; Jaiswal, V. K.; Nenov, A.; Garavelli, M. Hybrid QM/MM Approach for the Calculation of Excited States in Complex Environments. In *Comprehensive Computational Chemistry (First Edition)*; Yáñez, M., Boyd, R. J., Eds.; Elsevier: Oxford, 2024; pp 158–187. https://doi.org/10.1016/B978-0-12-821978-2.00059-3.
(42) Conti, I.; Bonfanti, M.; Nenov, A.; Rivalta, I.; Garavelli, M. Photo-Active Biological Molecular Materials: From Photoinduced Dynamics to Transient Electronic Spectroscopies. In *QM/MM Studies of Light-responsive Biological Systems*; Andruniów, T., Olivucci, M., Eds.; Springer International Publishing: Cham, 2021; pp 77–142. https://doi.org/10.1007/978-3-030-57721-6_2.
(43) Li Manni, G.; Fdez. Galván, I.; Alavi, A.; Aleotti, F.; Aquilante, F.; Autschbach, J.; Avagliano, D.; Baiardi, A.; Bao, J. J.; Battaglia, S.; Birnoschi, L.; Blanco-González, A.; Bokarev, S. I.; Broer, R.; Cacciari, R.; Calio, P. B.; Carlson, R. K.; Carvalho Couto, R.; Cerdán, L.; Chibotaru, L. F.; Chilton, N. F.; Church, J. R.; Conti, I.; Coriani, S.; Cuéllar-Zuquin, J.; Daoud, R. E.; Dattani, N.; Decleva, P.; de Graaf, C.; Delcey, M. G.; De Vico, L.; Dobrautz, W.; Dong, S. S.; Feng, R.; Ferré, N.; Filatov(Gulak), M.; Gagliardi, L.; Garavelli, M.; González, L.; Guan, Y.; Guo, M.; Hennefarth, M. R.; Hermes, M. R.; Hoyer, C. E.; Huix-Rotllant, M.; Jaiswal, V. K.; Kaiser, A.; Kaliakin, D. S.; Khamesian, M.; King, D. S.; Kochetov, V.; Krośnicki, M.; Kumaar, A. A.; Larsson, E. D.; Lehtola, S.; Lepetit, M.-B.; Lischka, H.; López Ríos, P.; Lundberg, M.; Ma, D.; Mai, S.; Marquetand, P.; Merritt, I. C. D.; Montorsi, F.; Mörchen, M.; Nenov, A.; Nguyen, V. H. A.; Nishimoto, Y.; Oakley, M. S.; Olivucci, M.; Oppel, M.; Padula, D.; Pandharkar, R.; Phung, Q. M.; Plasser, F.; Raggi, G.; Rebolini, E.; Reiher, M.; Rivalta, I.; Roca-Sanjuán, D.; Romig, T.; Safari, A. A.; Sánchez-Mansilla, A.; Sand, A. M.; Schapiro, I.; Scott, T. R.; Segarra-Martí, J.; Segatta, F.; Sergentu, D.-C.; Sharma, P.; Shepard, R.; Shu, Y.; Staab, J. K.; Straatsma, T. P.; Sørensen, L. K.; Tenorio, B. N. C.; Truhlar, D. G.; Ungur, L.; Vacher, M.; Veryazov, V.; Voß, T. A.; Weser, O.; Wu, D.; Yang, X.; Yarkony, D.; Zhou, C.; Zobel, J. P.; Lindh, R. The OpenMolcas Web: A Community-Driven Approach to Advancing Computational Chemistry. *J. Chem. Theory Comput.* **2023**. https://doi.org/10.1021/acs.jctc.3c00182.
(44) Frisch, M. J.; Trucks, G. W.; Schlegel, H. B.; Scuseria, G. E.; Robb, M. A.; Cheeseman, J. R.; Scalmani, G.; Barone, V.; Petersson, G. A.; Nakatsuji, H.; Li, X.; Caricato, M.; Marenich, A. V.; Bloino, J.; Janesko, B. G.; Gomperts, R.; Mennucci, B.; Hratch, D. J. Gaussian 16, 2016.
(45) Case, D. A.; Aktulga, H. M.; Belfon, K.; Ben-Shalom, I. Y.; Brozell, S. R.; Cerutti, D. S.; Cheatham, T.E., I.; Cisneros, G. A.; Cruziero, V. W. D.; Darden, T. A.; Duke, R. E.; Giambasu, G.; Gilson, M. K.; Gohlke, H.; Goetz, A. W.; Harris, R.; Izadi, S.; Izmailov, S. A.; Jin, C.; Kasavajhala, K.; Kaymak, M. C.; King, E.; Kovalenko, A.; Kurtzman, T.; Lee, T. S.; LeGrand, S.; Li, P.; Lin, C.; Liu, J.; Luchko, T.; Luo, R.; Machado, M.; Man, V.; Manathunga, M.; Merz, K. M.; Miao, Y.; Mikhailovskii, O.; Monard, G.; Nguyen, H.; O'Hearn, K. A.; Onufriev, A.; Pan, F.; Pantano, S.; Qi, R.; Rahnamoun, A.; Roe, D. R.; Roitberg, A.; Sagui, C.; Schott-Verdugo, S.; Shen, J.; Simmerling, C. L.; Skrynnikov, N. R.; Smith, J.; Swails, J.; Walker, R. C.; Wang, J.; Wei, H.; Wolf, R. M.; Wu, X.; Xue, Y.; York, D. M.; Zhao, S.; Kollman, P. A. Amber 2021, 2021.
(46) Avagliano, D.; Bonfanti, M.; Nenov, A.; Garavelli, M. Automatized Protocol and Interface to Simulate QM/MM Time-Resolved Transient Absorption at TD-DFT Level with COBRAMM. *Journal of Computational Chemistry* **2022**, *43* (24), 1641–1655. https://doi.org/10.1002/jcc.26966.

(47) Aidas, K.; Angeli, C.; Bak, K. L.; Bakken, V.; Bast, R.; Boman, L.; Christiansen, O.; Cimiraglia, R.; Coriani, S.; Dahle, P.; Dalskov, E. K.; Ekström, U.; Enevoldsen, T.; Eriksen, J. J.; Ettenhuber, P.; Fernández, B.; Ferrighi, L.; Fliegl, H.; Frediani, L.; Hald, K.; Halkier, A.; Hättig, C.; Heiberg, H.; Helgaker, T.; Hennum, A. C.; Hettema, H.; Hjertenæs, E.; Høst, S.; Høyvik, I.-M.; Iozzi, M. F.; Jansík, B.; Jensen, H. J. Aa.; Jonsson, D.; Jørgensen, P.; Kauczor, J.; Kirpekar, S.; Kjærgaard, T.; Klopper, W.; Knecht, S.; Kobayashi, R.; Koch, H.; Kongsted, J.; Krapp, A.; Kristensen, K.; Ligabue, A.; Lutnæs, O. B.; Melo, J. I.; Mikkelsen, K. V.; Myhre, R. H.; Neiss, C.; Nielsen, C. B.; Norman, P.; Olsen, J.; Olsen, J. M. H.; Osted, A.; Packer, M. J.; Pawlowski, F.; Pedersen, T. B.; Provasi, P. F.; Reine, S.; Rinkevicius, Z.; Ruden, T. A.; Ruud, K.; Rybkin, V. V.; Sałek, P.; Samson, C. C. M.; de Merás, A. S.; Saue, T.; Sauer, S. P. A.; Schimmelpfennig, B.; Sneskov, K.; Steindal, A. H.; Sylvester-Hvid, K. O.; Taylor, P. R.; Teale, A. M.; Tellgren, E. I.; Tew, D. P.; Thorvaldsen, A. J.; Thøgersen, L.; Vahtras, O.; Watson, M. A.; Wilson, D. J. D.; Ziolkowski, M.; Ågren, H. The Dalton Quantum Chemistry Program System. *WIREs Computational Molecular Science* **2014**, *4* (3), 269–284. https://doi.org/10.1002/wcms.1172.

(48) Steinmann, C.; Reinholdt, P.; Nørby, M. S.; Kongsted, J.; Olsen, J. M. H. Response Properties of Embedded Molecules through the Polarizable Embedding Model. *International Journal of Quantum Chemistry* **2019**, *119* (1), e25717. https://doi.org/10.1002/qua.25717.

(49) Beerepoot, M. T. P.; Steindal, A. H.; List, N. H.; Kongsted, J.; Olsen, J. M. H. Averaged Solvent Embedding Potential Parameters for Multiscale Modeling of Molecular Properties. *J. Chem. Theory Comput.* **2016**, *12* (4), 1684–1695. https://doi.org/10.1021/acs.jctc.5b01000.

(50) Tavernelli, I.; Curchod, B. F. E.; Laktionov, A.; Rothlisberger, U. Nonadiabatic Coupling Vectors for Excited States within Time-Dependent Density Functional Theory in the Tamm–Dancoff Approximation and Beyond. *The Journal of Chemical Physics* **2010**, *133* (19), 194104. https://doi.org/10.1063/1.3503765.

(51) Herbert, J. M.; Zhang, X.; Morrison, A. F.; Liu, J. Beyond Time-Dependent Density Functional Theory Using Only Single Excitations: Methods for Computational Studies of Excited States in Complex Systems. *Acc. Chem. Res.* **2016**, *49* (5), 931–941. https://doi.org/10.1021/acs.accounts.6b00047.

(52) Casanova, D.; Krylov, A. I. Spin-Flip Methods in Quantum Chemistry. *Phys. Chem. Chem. Phys.* **2020**, *22* (8), 4326–4342. https://doi.org/10.1039/C9CP06507E.

(53) Shao, Y.; Head-Gordon, M.; Krylov, A. I. The Spin–Flip Approach within Time-Dependent Density Functional Theory: Theory and Applications to Diradicals. *The Journal of Chemical Physics* **2003**, *118* (11), 4807–4818. https://doi.org/10.1063/1.1545679.

(54) Martínez-Fernández, L.; Pepino, A. J.; Segarra-Martí, J.; Jovaišaitė, J.; Vaya, I.; Nenov, A.; Markovitsi, D.; Gustavsson, T.; Banyasz, A.; Garavelli, M.; Improta, R. Photophysics of Deoxycytidine and 5-Methyldeoxycytidine in Solution: A Comprehensive Picture by Quantum Mechanical Calculations and Femtosecond Fluorescence Spectroscopy. *J. Am. Chem. Soc.* **2017**, *139* (23), 7780–7791. https://doi.org/10.1021/jacs.7b01145.

(55) Barbatti, M.; Lan, Z.; Crespo-Otero, R.; Szymczak, J. J.; Lischka, H.; Thiel, W. Critical Appraisal of Excited State Nonadiabatic Dynamics Simulations of 9H-Adeninea). *The Journal of Chemical Physics* **2012**, *137* (22), 22A503. https://doi.org/10.1063/1.4731649.

(56) Clark, L. B.; Peschel, G. G.; Tinoco, I. Jr. Vapor Spectra and Heats of Vaporization of Some Purine and Pyrimidine Bases1. *J. Phys. Chem.* **1965**, *69* (10), 3615–3618. https://doi.org/10.1021/j100894a063.
(57) Ploeser, J. McT.; Loring, H. S. THE ULTRAVIOLET ABSORPTION SPECTRA OF THE PYRIMIDINE RIBONUCLEOSIDES AND RIBONUCLEOTIDES. *Journal of Biological Chemistry* **1949**, *178* (1), 431–437. https://doi.org/10.1016/S0021-9258(18)56973-8.
(58) Sprecher, C. A.; Johnson Jr., W. C. Circular Dichroism of the Nucleic Acid Monomers. *Biopolymers* **1977**, *16* (10), 2243–2264. https://doi.org/10.1002/bip.1977.360161012.
(59) Kánnár, D.; Szalay, P. G. Benchmarking Coupled Cluster Methods on Singlet Excited States of Nucleobases. *Journal of Molecular Modeling* **2014**, *20* (11), 2503. https://doi.org/10.1007/s00894-014-2503-2.
(60) Epifanovsky, E.; Kowalski, K.; Fan, P.-D.; Valiev, M.; Matsika, S.; Krylov, A. I. On the Electronically Excited States of Uracil. *J. Phys. Chem. A* **2008**, *112* (40), 9983–9992. https://doi.org/10.1021/jp803758q.
(61) Bondanza, M.; Nottoli, M.; Cupellini, L.; Lipparini, F.; Mennucci, B. Polarizable Embedding QM/MM: The Future Gold Standard for Complex (Bio)Systems? *Phys. Chem. Chem. Phys.* **2020**, *22* (26), 14433–14448. https://doi.org/10.1039/D0CP02119A.
(62) Loco, D.; Lagardère, L.; Caprasecca, S.; Lipparini, F.; Mennucci, B.; Piquemal, J.-P. Hybrid QM/MM Molecular Dynamics with AMOEBA Polarizable Embedding. *J. Chem. Theory Comput.* **2017**, *13* (9), 4025–4033. https://doi.org/10.1021/acs.jctc.7b00572.
(63) Olsen, J. M. H.; Kongsted, J. Chapter 3 - Molecular Properties through Polarizable Embedding. In *Advances in Quantum Chemistry*; Sabin, J. R., Brändas, E., Eds.; Academic Press, 2011; Vol. 61, pp 107–143. https://doi.org/10.1016/B978-0-12-386013-2.00003-6.
(64) List, N. H.; Olsen, J. M. H.; Kongsted, J. Excited States in Large Molecular Systems through Polarizable Embedding. *Phys. Chem. Chem. Phys.* **2016**, *18* (30), 20234–20250. https://doi.org/10.1039/C6CP03834D.
(65) Cammi, R.; Corni, S.; Mennucci, B.; Tomasi, J. Electronic Excitation Energies of Molecules in Solution: State Specific and Linear Response Methods for Nonequilibrium Continuum Solvation Models. *The Journal of Chemical Physics* **2005**, *122* (10), 104513. https://doi.org/10.1063/1.1867373.
(66) Guido, C. A.; Chrayteh, A.; Scalmani, G.; Mennucci, B.; Jacquemin, D. Simple Protocol for Capturing Both Linear-Response and State-Specific Effects in Excited-State Calculations with Continuum Solvation Models. *J. Chem. Theory Comput.* **2021**, *17* (8), 5155–5164. https://doi.org/10.1021/acs.jctc.1c00490.
(67) Zazza, C.; Olsen, J. M.; Kongsted, J. Solvatochromic Shifts vs Nanosolvation Patterns: Uracil in Water as a Test Case. *Computational and Theoretical Chemistry* **2011**, *974* (1), 109–116. https://doi.org/10.1016/j.comptc.2011.07.020.
(68) Zuehlsdorff, T. J.; Isborn, C. M. Modeling Absorption Spectra of Molecules in Solution. *International Journal of Quantum Chemistry* **2019**, *119* (1), e25719. https://doi.org/10.1002/qua.25719.
(69) Improta, R.; Barone, V.; Scalmani, G.; Frisch, M. J. A State-Specific Polarizable Continuum Model Time Dependent Density Functional Theory Method for Excited State Calculations in Solution. *The Journal of Chemical Physics* **2006**, *125* (5), 054103. https://doi.org/10.1063/1.2222364.

(70) Gil, G.; Pipolo, S.; Delgado, A.; Rozzi, C. A.; Corni, S. Nonequilibrium Solvent Polarization Effects in Real-Time Electronic Dynamics of Solute Molecules Subject to Time-Dependent Electric Fields: A New Feature of the Polarizable Continuum Model. *J. Chem. Theory Comput.* **2019**, *15* (4), 2306–2319. https://doi.org/10.1021/acs.jctc.9b00010.
(71) Olsen, J. M.; Aidas, K.; Mikkelsen, K. V.; Kongsted, J. Solvatochromic Shifts in Uracil: A Combined MD-QM/MM Study. *J. Chem. Theory Comput.* **2010**, *6* (1), 249–256. https://doi.org/10.1021/ct900502s.
(72) DeFusco, A.; Ivanic, J.; Schmidt, M. W.; Gordon, M. S. Solvent-Induced Shifts in Electronic Spectra of Uracil. *J. Phys. Chem. A* **2011**, *115* (18), 4574–4582. https://doi.org/10.1021/jp112230f.
(73) Giussani, A.; Segarra-Martí, J.; Nenov, A.; Rivalta, I.; Tolomelli, A.; Mukamel, S.; Garavelli, M. Spectroscopic Fingerprints of DNA/RNA Pyrimidine Nucleobases in Third-Order Nonlinear Electronic Spectra. *Theoretical Chemistry Accounts* **2016**, *135* (5), 121. https://doi.org/10.1007/s00214-016-1867-z.
(74) Cohen, B.; Hare, P. M.; Kohler, B. Ultrafast Excited-State Dynamics of Adenine and Monomethylated Adenines in Solution: Implications for the Nonradiative Decay Mechanism. *J. Am. Chem. Soc.* **2003**, *125* (44), 13594–13601. https://doi.org/10.1021/ja035628z.

FIGURE CAPTIONS

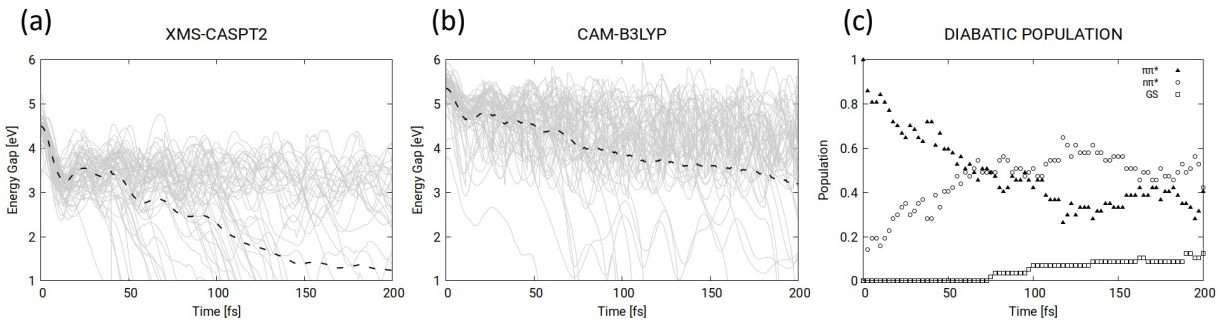

610

611 **Figure 1**. Energy-gap of the active-state with the ground-state along time during surface-
612 hopping simulations at XMS-CASPT2 (a) and TD-DFT/CAM-B3LYP (b). The average energy-
613 gap is shown with dashed black line. The TD-DFT computations suffer from SCF convergence
614 issues in regions of energy degeneracy with ground-state, so the trajectories have been stopped
615 around the S1/S0 conical intersections and have been assumed to hop to ground-state. (c) Time-
616 evolution of average population of diabatic states $n\pi^*$/ $\pi\pi^*$/GS in TD-DFT(QM/MM)
617 dynamics.

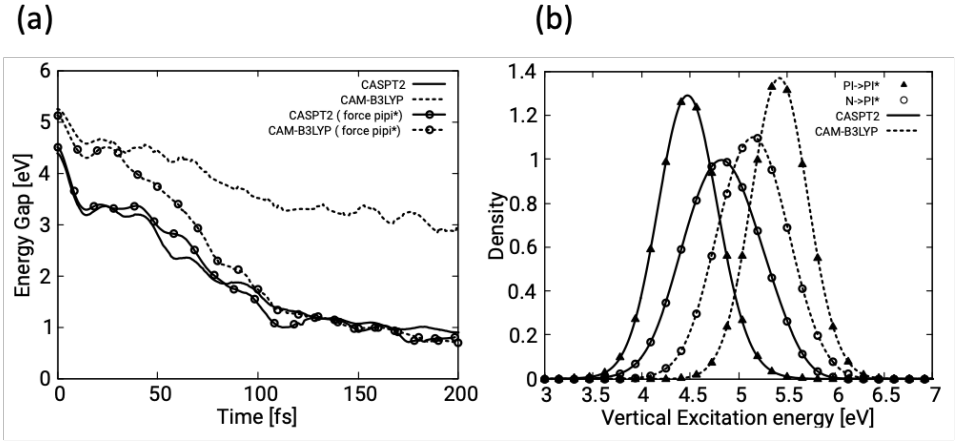

618

619 **Figure 2.** (a) Time-evolution of average energy-gap of active-state w.r.t. ground-state in
620 CASPT2(QM/MM) and TD-DFT(QM/MM) dynamics for a subset of 29 trajectories from
621 Figure 1. (b) Distribution of vertical transition energies of $\pi\pi^*$/ $n\pi^*$ states for 500 solvated
622 structures in the wigner ensemble for CASPT2 and TD-DFT in the QM/MM setup.

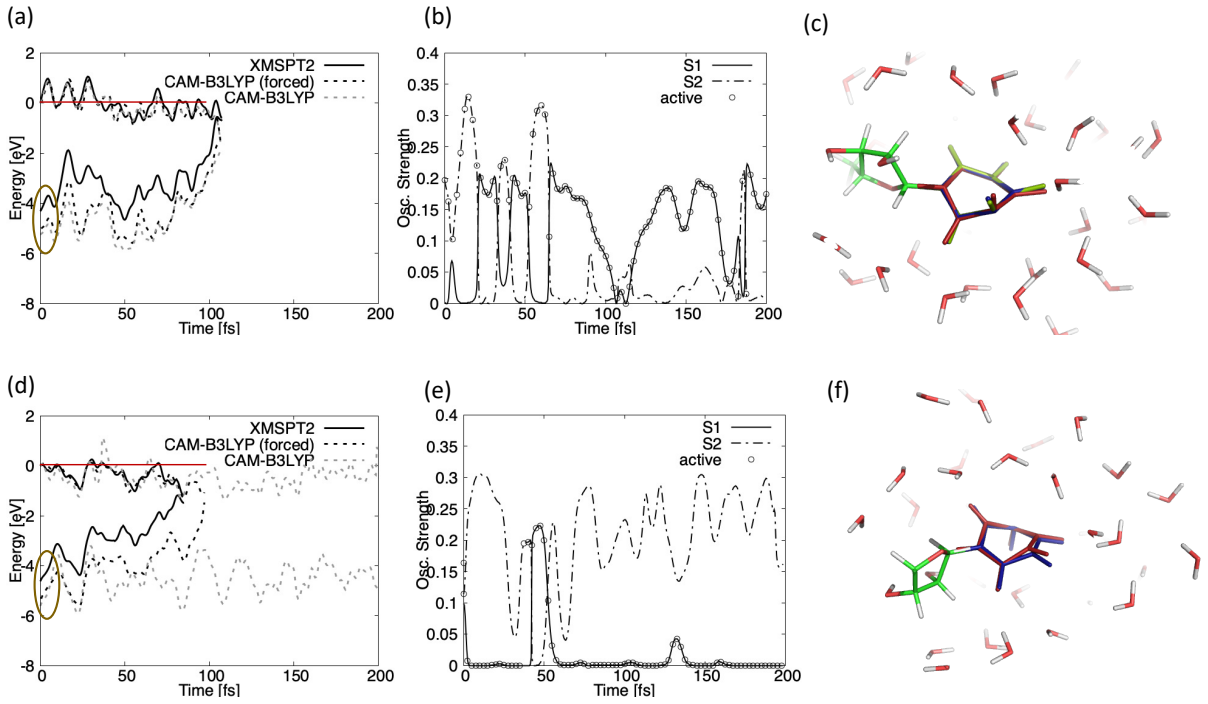

Figure 3. Comparison of dynamics where unbiased TD-DFT hops to the ground-state (a,b,c) or remains trapped in $n\pi^*$ excited-state (d,e,f). (a,d) Potential energies of active-state and the ground-state at XMS-CASPT2, unbiased TD-DFT, and TD-DFT forced on the $\pi\pi^*$ state. The red line has been added at the ππ* energy at t=0 to guide the reader to appreciate the similar dynamical fluctuations in the energies observed at CASPT2 and TDDFT. The rigid shift of excited-state PES w.r.t. the ground-state at Franck-Condon is shown by the brown circle at t=0 (b,e) Oscillator strength of the active state in unbiased TD-DFT dynamics. (c,d) molecular structures of conical intersections at hopping times for the dynamics. All 29 trajectories with population constrained on $\pi\pi^*$state at SS-CASPT2/TDDFT level are shown in Figure S1.

	$\pi\pi^*$	$n\pi^*$	$\pi\pi^*$	$n\pi^*$
VACUUM	5.229	4.815		
	QM-REGION= NUCLEOTIDE (BASE+SUGAR)		QM-REGION=NUCLEOTIDE + H-bonded waters	
EEmbedding[a]	5.347	5.290	5.267	5.279
EEmbedding[b]	5.319	5.211	5.264	5.238
PolEmbedding	5.276	5.457	5.231	5.339
PCM – 0th order	5.264	5.146	5.251	5.408
PCM - LR	5.208	5.144	5.201	5.407
PCM -cLR	5.252	5.080	5.241	5.359
PCM – cLR2	5.196	5.075	5.191	5.358

Table1 Energies of the $\pi\pi^*$ and $n\pi^*$ state computed at CAM-B3LYP/cc-pVTZ level at Franck-Condon geometry (optimized at MP2/EEmbedding (TIP3P) level) in two different QM-regions and various methods for solvent description. Grey background highlight the QM/MM setups showing the np* state higher than pp*, as expected in polar environments. All schemes have been repeated for two basis-sets as shown in the table. All reported vertical transition energies are in eV.

[a] Electrostatic Embedding using solvent charges of TIP3P model,.

[b] Electrostatic Embedding using solvent charges of SEP model from Pyframe.